2014

An Interconnection and Damping Assignment Passivity-Based Controller for a DC–DC Boost Converter With a Constant Power Load

Jianwu Zeng
University of Nebraska-Lincoln, jzeng@huskers.unl.edu

Zhe Zhang
University of Nebraska-Lincoln, zhang.zhe@huskers.unl.edu

Wei Qiao
University of Nebraska-Lincoln, wqiao@engr.unl.edu

Pages: 2314 – 2322, DOI: 10.1109/TIA.2013.2290872

An Interconnection and Damping Assignment Passivity-Based Controller for a DC–DC Boost Converter With a Constant Power Load

Jianwu Zeng, *Student Member, IEEE*, Zhe Zhang, *Student Member, IEEE*, and Wei Qiao, *Senior Member, IEEE*

***Abstract*—This paper proposes an adaptive interconnection and damping assignment (IDA) passivity-based controller (PBC) with a complementary proportional integral (PI) controller for dc–dc boost converters with constant power loads (CPLs). The plant is modeled as a port-controlled Hamiltonian system (PCHS). A virtual circuit that interprets the parameters of the PCHS is then derived to determine the parameters of the IDA-PBC for the system to work in the underdamping, critical-damping, and overdamping modes. Moreover, a complementary PI controller is designed to eliminate the steady-state output voltage error of the IDA-PBC caused by the load variation. Simulation studies are carried out in MATLAB/Simulink to validate the proposed control algorithm for a dc–dc boost converter with a CPL; results show that the proposed control algorithm ensures the stability and fast response of the system in different modes when the load changes. Experimental results are provided to further validate the design and simulation of the proposed control algorithm.**

***Index Terms*—Constant power load (CPL), dc–dc boost converter, interconnection and damping assignment (IDA), passivity-based controller (PBC), port-controlled Hamiltonian system (PCHS).**

I. Introduction

With the growth of energy demand and depletion of energy resources, renewable energy has drawn more and more attention [1]. In recent years, many distributed renewable energy resources, such as photovoltaic (PV) systems and wind turbines, are being installed into the utility power grids. However, the integration of many distributed generation units may affect the power quality of the utility grids [2]. One solution to the problem is to construct a microgrid to integrate the distributed generation units in a certain area, manage the units locally within the microgrid, and connect the microgrid to the utility grid while satisfying the power quality requirement at the connecting point of the microgrid.

There are two categories of microgrids, namely, ac microgrids and dc microgrids. Most microgrids adopt ac distribution, which is the same as the utility power grids. In this case, the dc power sources, such as PV systems, fuel cells, and energy storage systems, are connected to the microgrids via inverters. DC microgrids have been proposed and researched in order to reduce energy conversion losses from the sources to dc loads [3], [4]. Moreover, the proliferation of low-power electronic devices and the potential of using light-emitting diodes to reduce lighting loads make it plausible to use dc microgrids [5]. The technical challenges associated with the operation and control of dc microgrids is immense [6], particularly when a dc microgrid with constant power loads (CPLs) works in the island mode.

In a dc microgrid, dc sources are commonly connected to the grid through dc–dc boost converters [7]. It is well known that the negative incremental impedance property of a CPL might cause a dc-bus voltage oscillation or even instability when conventional linear controllers are used [8]. Much research effort has been devoted to developing nonlinear control techniques for converters with CPLs [9]. For example, a sliding-mode controller was developed for a buck converter with a CPL [10]; a hybrid model predictive control was proposed for a boost converter with a CPL [11]; a passivity-based controller (PBC) was designed for buck, boost, and buck–boost converters with CPLs [12], [13]. An advantage of the PBC over other nonlinear control methods is that this approach utilizes the structural properties of the physical systems to achieve an easily implemented control law [14].

The PBC combined with the interconnection and damping assignment (IDA) technique has been used for stability analysis of a dc microgrid [15]. However, the IDA parameters were usually determined by simulations and fixed after they were designed for a typical operating condition, e.g., a specific power level of the CPL and dc-bus voltage. In real applications, the values of system state variables usually vary from time to time. Therefore, the IDA with fixed parameters will not be optimal when the system operating condition changes. Furthermore, the PBC requires precise values of the state variables in order to control the system to work at a desired operating point. However, estimation or measurement errors of the state variables may result in a deviation between the real and desired operating points when using a PBC.

Manuscript received February 11, 2013; revised August 23, 2013; accepted November 2, 2013. Date of publication November 13, 2013; date of current version July 15, 2014. Paper 2013-IACC-112.R1, presented at the 2012 IEEE Industry Applications Society Annual Meeting, Las Vegas, NV, USA, October 7–11, and approved for publication in the IEEE Transactions on Industry Applications by the Industrial Automation and Control Committee of the IEEE Industry Applications Society. This work was supported in part by the U.S. Federal Highway Administration under Agreement DTFH61-10-H-00003. Any opinions, findings, and conclusions or recommendations expressed in this publication are those of the authors and do not necessarily reflect the view of the Federal Highway Administration.

The authors are with the Power and Energy Systems Laboratory, Department of Electrical Engineering, University of Nebraska–Lincoln, Lincoln, NE 68588-0511 USA (e-mail: jzeng@huskers.unl.edu; zhang.zhe@huskers.unl.edu; wqiao@engr.unl.edu).

Color versions of one or more of the figures in this paper are available online at http://ieeexplore.ieee.org.

Digital Object Identifier 10.1109/TIA.2013.2290872

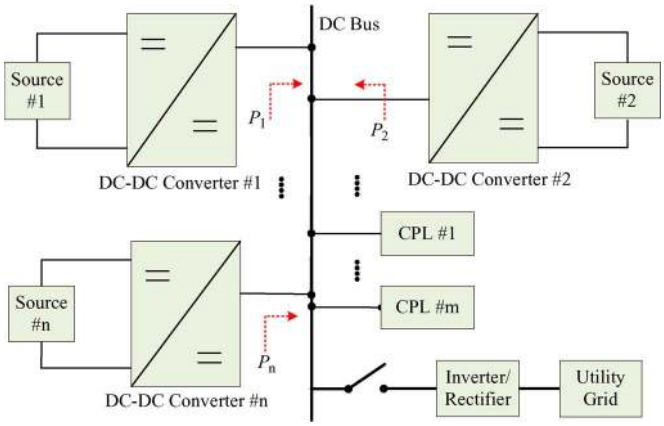

Fig. 1. Typical configuration of a dc microgrid.

This paper proposes an adaptive IDA-PBC for a dc–dc boost converter with a CPL. By using the principles of the port-controlled Hamiltonian system (PCHS) and IDA, a virtual circuit is derived for designing the parameters of the proposed controller. Then, three different working modes, i.e., under-damping, critical-damping, and overdamping modes, of the dc–dc boost converter with a CPL can be achieved by setting proper controller parameters through analyzing the virtual circuit. Moreover, since the dc–dc boost converter exhibits highly nonlinear properties, it is not an easy task to design a control algorithm that is robust against load variations [16]. In this paper, a complementary proportional integral (PI) controller is designed to work with the IDA-PBC together to eliminate the steady-state error of the output voltage caused by the load variation.

This paper is organized as follows. Section II introduces the typical structure of a dc microgrid with dc–dc converter integrated sources and describes the passivity model of a dc–dc boost converter. Section III proposes the PI controller-compensated IDA-PBC for controlling the dc–dc boost converter with a CPL. Section IV validates the proposed control algorithm by computer simulations in MATLAB/Simulink. Section V further validates the proposed control algorithm by experiments. Concluding remarks are provided in Section VI to summarize this paper.

II. Problem Description

A. DC Microgrid With CPLs

Fig. 1 shows the typical configuration of a dc microgrid, which consists of n sources and m CPLs. Each source is connected to the microgrid through a dc–dc converter. The dc microgrid is connected to the utility grid through a rectifier/inverter interface. When the dc microgrid works in the grid-connected mode, the utility grid not only provides the deficient power required by the dc microgrid but also absorbs the surplus power generated by the microgrid. However, when the dc microgird is disconnected from the utility grid, it will become an autonomic system and operate in the island mode. In this case, the dc microgrid will suffer from two issues. One is the unbalance power between the sources and loads. The other is dc-bus voltage variations. These two issues will become more challenging when the microgrid has CPLs. The CPLs may cause power oscillation or even instability of the system because of their negative impedance characteristics [6], which cannot be stabilized by using conventional linear control methods [17]. To overcome the instability problem, nonlinear controllers are required [18].

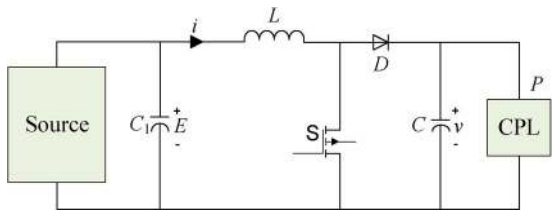

Fig. 2. DC–DC boost converter with a CPL.

In this paper, it is assumed that the microgrid adopts a two-level control scheme, namely, the grid-level control and the converter-level control. The grid-level controller assigns a power reference for each converter (see Fig. 1), in which P_i $(i = 1, 2, \ldots, n)$ is the reference power for the ith converter. The converter-level controller regulates the converter output power to its reference value assigned by the grid-level controller. The focus of this paper is to design the converter-level controller for each dc–dc converter, so that it is capable of supplying desired power while keeping the dc-bus voltage at a desired constant value. Particularly, when there is only one source available to supply the dc microgrid operating in the island mode, then the overall load in the microgrid will be viewed as a CPL for the dc–dc converter of the source. For example, when all of the renewable energy sources are unavailable or only generate a little power, the CPLs of the dc microgrid are all supplied by a backup energy storage system, e.g., a battery system.

B. Modeling a DC–DC Boost Converter With a CPL

Fig. 2 shows the topology of a dc–dc boost converter supplying a CPL. To simplify the analysis, it is assumed that the boost converter works in the continuous conduction mode. The differential equations of the circuit can be expressed as

$$\begin{cases} \dot{i} = \frac{-(1-d)}{L} v + \frac{E}{L} \\ \dot{v} = \frac{1-d}{C} i - \frac{P}{C \cdot v} \end{cases} \tag{1}$$

where i is the inductor current; v is the converter output voltage or the voltage of the dc bus at the load side; d is the duty ratio of the switch $(0 \leq d \leq 1)$; P is the power of the CPL; and E is the input voltage of the boost converter.

It has been proved [10], [19] that due to the CPL's negative incremental impedance characteristic, the system in Fig. 2 cannot be stabilized by using traditional linear controllers, e.g., a PI controller with fixed parameters, during large disturbances or changes in the operating condition, e.g., a large variation in the dc-bus voltage or the load power.

III. Design of the Proposed Control Algorithm

In this section, an improved IDA-PBC is proposed for the dc–dc boost converter with a CPL (see Fig. 2), which is

modeled in a PCHS form. The proposed nonlinear controller ensures the stability and fast response of the system during large disturbances in load and dc-bus voltage.

A. IDA-PBC

From the energy point of view, the Hamiltonian function of the dc–dc boost converter with a CPL represents the total energy stored in the dynamic system and can be written as

$$H(x) = \frac{1}{2L}\, x_1^2 + \frac{1}{2C}\, x_2^2 \tag{2}$$

where $x = [x_1, x_2]^T = [L \cdot i, C \cdot v]^T$ represents the inductor flux linkage and the electric charge in the capacitor. Considering (1) and (2), the boost converter with a CPL can be modeled in a PCHS form as

$$\begin{cases} \dot{x} = [J(x) - R(x)] \cdot \frac{\partial H(x)}{\partial x} + \zeta + g(x)u \\ y = g^T(x) \frac{\partial H(x)}{\partial x} \end{cases} \tag{3}$$

where $J(x)$ is the interconnection matrix satisfying $J(x) = -J(x)$; $R(x)$ is the dissipation matrix satisfying $R(x) = R^T(x)$; $\zeta = [E, 0]^T$ is the input voltage term representing the external force; u is the control signal; and y is the output of the PCHS. The coefficient matrices and vector are expressed as

$$J(x) = \begin{pmatrix} 0 & -1 \\ 1 & 0 \end{pmatrix}$$

$$R(x) = \begin{pmatrix} 0 & 0 \\ 0 & \frac{PC}{x_2^2} \end{pmatrix}$$

$$g(x) = \begin{pmatrix} \frac{x_2}{C} \\ \frac{-x_1}{L} \end{pmatrix}.$$

The idea of the IDA is to assign a desired energy function to the system with a desired equilibrium point x^* via modifying the interconnection and dissipation matrices and the control law (called reshaping). In this paper, the desired energy function is defined as follows:

$$H_d(x) = \frac{1}{2L}\,(x_1 - x_1^*)^2 + \frac{1}{2C}\,(x_2 - x_2^*)^2. \tag{4}$$

Assume that there are matrices $J_d(x) = -J_d^T(x)$, $R_d(x) = R_d^T(x) \geq 0$, and a differentiable scalar function $H_d(x)$ such that

$$x^* = \arg\min H_d(x). \tag{5}$$

Then assume that there exists a control law $u = \beta(x)$ making the closed-loop system (3) take the following PCHS form:

$$\dot{x} = [J_d(x) - R_d(x)] \cdot \frac{\partial H_d(x)}{\partial x} \tag{6}$$

with a stable equilibrium x^*. Furthermore, if the largest invariant set of x of the closed-loop system contained in the following set:

$$\left\{ x \in R^n \mid \frac{\partial H_d^T(x)}{\partial x}\, R_d(x) \frac{\partial H_d(x)}{\partial x} = 0 \right\} \tag{7}$$

is equal to $\{x^*\}$, the closed-loop system is asymptotically stable [20].

Proof: It is known that the PCHS naturally satisfies the energy-balance criteria, which is of the form, i.e.,

$$\dot{H} = u^T y - \frac{\partial H^T(x)}{\partial x}\, R(x) \frac{\partial H(x)}{\partial x}. \tag{8}$$

By substituting $u = \beta(x)$ into (3), (6) can be obtained. Since there is no input port in the PCHS described by (6) after the reshaping process, the following can be obtained along the states' trajectories of the closed-loop system (6):

$$\dot{H}_d = -\frac{\partial H_d^T(x)}{\partial x}\, R_d(x) \frac{\partial H_d(x)}{\partial x} \leq 0. \tag{9}$$

Since $R_d(x)$ is a positive-definite matrix and $H_d(x)$ is nonincreasing along with time, $H_d(x)$ is qualified as Lyapunov function. Asymptotic stability follows immediately by invoking La Salle's invariance principle [21] and condition (7).

Then, the desired target dynamics of the PCHS is (6) by defining $J_d(x) = 0$ and $R_d(x) = \mathrm{diag}(r_1, 1/r_2)$, where $\mathrm{diag}(\cdot)$ denotes a diagonal matrix. According to (3) and (6) there is

$$[J_d(x) - R_d(x)] \frac{\partial H_d(x)}{\partial x} = [J(x) - R(x)] \frac{\partial H(x)}{\partial x} + \zeta + g(x)u. \tag{10}$$

Let $H_d(x) = H(x) + H_a(x)$, $J_d(x) = J(x) + J_a(x) + g(x)u \cdot [\partial H/\partial x]^{-1}$, $R_d(x) = R(x) + R_a(x)$, and $u = d$, which is the duty ratio of the switch, then

$$[J_d(x) - R_d(x)] \frac{\partial H_a(x)}{\partial x} = -[J_a(x) - R_a(x)] \frac{\partial H(x)}{\partial x} + \zeta \tag{11}$$

where

$$J_a(x) = -\begin{pmatrix} 0 & -(1-d) \\ 1-d & 0 \end{pmatrix}$$

$$R_a(x) = \begin{pmatrix} r_1 & 0 \\ 0 & \frac{1}{r_2} - \frac{C^2 P}{x_2^2} \end{pmatrix}.$$

Equation (11) can be further written as

$$\begin{pmatrix} -r_1 & 0 \\ 0 & \frac{-1}{r_2} \end{pmatrix} \frac{\partial H_a(x)}{\partial x} = \begin{pmatrix} \frac{r_1}{L} & \frac{-(1-d)}{C} \\ \frac{(1-d)}{L} & \frac{1}{r_2 C} - \frac{CP}{x_2^2} \end{pmatrix} \cdot x + \begin{pmatrix} 1 \\ 0 \end{pmatrix} \cdot E. \tag{12}$$

Let $K(x) = (\partial H_a(x))/(\partial x) = ((\partial H_d(x))/(\partial x)) - ((\partial H(x))/(\partial x)) = [-(x_1^*/L) \quad -(x_2^*/C)]^T$, then (12) becomes

$$\begin{cases} -\frac{x_1^*}{L}\, r_1 = -\frac{r_1}{L}\, x_1 + \frac{1-d}{C}\, x_2 - E \\ -\frac{x_2^*}{C}\, \frac{1}{r_2} = \frac{-(1-d)}{L}\, x_1 - \frac{1}{r_2 \cdot C}\, x_2 + \frac{CP}{x_2}. \end{cases} \tag{13}$$

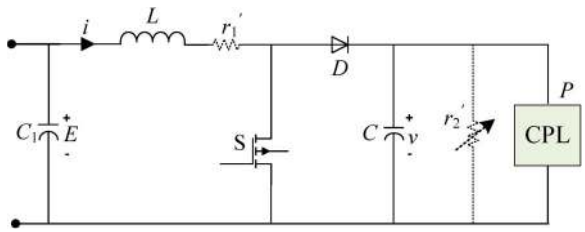

Fig. 3. Virtual equivalent circuit described by the right-hand side of (11).

Substituting $x = [L \cdot i, C \cdot v]^T$ into (13) yields

$$-I^* r_1 = -i \cdot r_1 + v(1-d) - E \tag{14}$$

$$\frac{-V^*}{r_2} = -i(1-d) - \frac{v}{r_2} + \frac{P}{v} \tag{15}$$

where I^* and V^* are the desired equilibrium points of i and v, respectively. Let $I^* = P/E$, the control law can be obtained from (14) as follows:

$$d = \frac{v - E + r_1(P/E - i)}{v} \tag{16}$$

when $i = I^*$, $d = 1 - E/v$. According to (1), there is $(1-d)i = C\,\dot{v} + P/v$. Then (15) becomes

$$\frac{1}{r_2} = \frac{C\dot{v}}{V^* - v}. \tag{17}$$

Equation (17) indicates that r_2 varies with the dc-bus voltage.

B. Damping Parameter Design

A new boost converter (see Fig. 3) is constructed by placing r_1' in series with the inductor and r_2' in parallel with the load in the original boost converter shown in Fig. 2. The function of r_1' and r_2' is to increase the damping factor of the circuit.

The state–space equation of the virtual equivalent circuit is

$$\dot{x} = \begin{pmatrix} -\frac{r_1'}{L} & -\frac{1-d}{C} \\ \frac{1-d}{L} & -\frac{1}{r_2' C} - \frac{CP}{x_2^2} \end{pmatrix} \cdot x + \begin{pmatrix} 1 \\ 0 \end{pmatrix} \cdot E \tag{18}$$

where the right-hand side of (18) has the same form as that of (12). Then, the virtual equivalent circuit in Fig. 3 can be used to determine the control parameter r_1 in (16) if the relationships between r_1 and r_1' as well as between r_2 and r_2' are known.

The desired state–space equation is shown as (6), which has the following form:

$$\dot{x} = [J_d(x) - R_d(x)] \cdot \frac{\partial H}{\partial x} = -\begin{bmatrix} r_1 & 0 \\ 0 & 1/r_2 \end{bmatrix} \cdot \begin{bmatrix} x_1 - x_1^* \\ x_2 - x_2^* \end{bmatrix}. \tag{19}$$

Since the virtual circuit has the same structure and dynamics as the desired system. Thus, the right-hand side of (18) and (19) should be the same. Therefore, the following equations can be obtained:

$$\begin{cases} r_1' = \frac{E + i r_1 - I^* r_1 - (1-d)v}{i}, & i > \varepsilon \\ \frac{1}{r_2'} = \frac{1}{r_2}\left(1 - \frac{V^*}{v}\right) + \frac{(1-d)i}{v} - \frac{P}{v^2}, & v \geq E \end{cases} \tag{20}$$

where ε represents a small positive value. Since $E - i \cdot r_1$ is the average voltage across switch S whose value is equal to $(1-d)v$. Then,

$$\begin{cases} r_1' = \left(2 - \frac{I^*}{i}\right) \cdot r_1, & i > \varepsilon \\ \frac{1}{r_2'} = \frac{(1-d)i - C \cdot \dot{v} - P/v}{v}, & v \geq E. \end{cases} \tag{21}$$

It can be seen that the control parameter r_1 varies with the current i if r_1' is fixed.

The characteristic equation of (18) becomes

$$s^2 + \left(\frac{r_1'}{L} + \frac{1}{r_2' C} + \frac{P}{CV^{*2}}\right) \cdot s + \frac{(1-D)^2}{LC} + \frac{r_1'}{L}\left(\frac{1}{r_2' C} + \frac{P}{CV^{*2}}\right) = 0 \tag{22}$$

where D is the steady-state duty ratio. The damping factor can be derived as follows:

$$\xi = \frac{\frac{r_1'}{L} + \frac{1}{C}\left(\frac{1}{r_2'} + \frac{P}{V^{*2}}\right)}{2\sqrt{\frac{(1-D)^2}{LC} + \frac{r_1'}{LC}\left(\frac{1}{r_2'} + \frac{P}{V^{*2}}\right)}}. \tag{23}$$

From (21), it can be seen that near the steady state when $v = V^*$ and $i = I^*$, there are $r_1' = r_1$ and $r_2' \to \infty$. Then the damping factor near the steady state becomes

$$\xi = \frac{\frac{r_1'}{L} + \frac{P}{CV^{*2}}}{2\sqrt{\frac{(1-D)^2}{LC} + \frac{r_1'}{LC} \cdot \frac{P}{V^{*2}}}}. \tag{24}$$

When $\xi \in (0, 1)$, the overshoot of the system can be calculated as

$$\sigma\% = \exp\left(-\frac{\pi \cdot \xi}{\sqrt{1-\xi^2}}\right) \times 100\%. \tag{25}$$

Particularly when $\xi = 1$, the critical value of r_1' becomes

$$r_{1C}' = 2\sqrt{\frac{L}{C}}(1-D) + \frac{LP}{CV^{*2}}. \tag{26}$$

Once the desired point $[V^*, I^*]$ is given, parameter r_1' can be calculated according to (24) if ξ is given. The control parameter r_1 in (16) then can be determined from (21).

C. Complementary PI Controller

Theoretically, the converter output voltage can be controlled at the desired value accurately by the proposed IDA-PBC if an accurate system dynamical model and accurate information of the system operating condition are available. However, in practice, due to the variations and uncertainties of system parameters and operating condition, e.g., the unmodeled parasitic impedance of the converter, the IDA-PBC may not be able to control the converter output voltage at the desired value exactly when the load power changes, resulting in a steady-state output voltage error e_v ($e_v = V^* - v$). To eliminate the steady-state error e_v, a complementary PI controller is designed to adjust the reference power of the IDA-PBC. Fig. 4 shows the overall

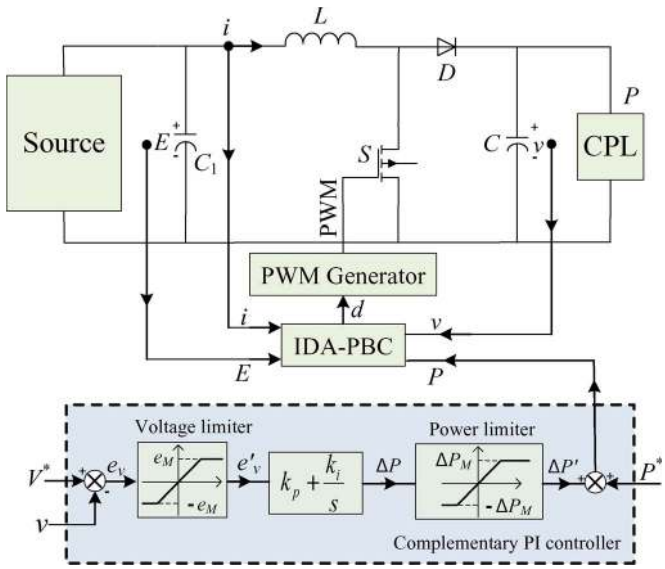

Fig. 4. Overall control algorithm of the system.

control scheme of the system. The complementary PI controller uses the output voltage of the converter as the feedback signal, which is compared with the desired output voltage. The voltage error is passed through a voltage limiter with the slop of one. The output of the voltage limiter, e'_v, is then used by a PI regulator to generate a compensating power reference ΔP as follows:

$$\Delta P = k_p \cdot e'_v + \int k_i \cdot e'_v \cdot dt \quad |e'_v| \le e_M \tag{27}$$

where e_M is the maximum value of the voltage limiter; k_p and k_i are the proportional and integral gains, respectively, of the PI regulator.

The value of ΔP is limited by a power limiter, whose output $\Delta P'$ is used as a supplementary power reference for the IDA-PBC to account for load variations. Then the power in (16) is adjusted as follows:

$$P = P^* + \Delta P' \quad |\Delta P'| \le \Delta P_M \tag{28}$$

where P^* is the reference power; P is the adjusted power value used in (16) and an input for the IDA-PBC; and ΔP_M is the maximum value of the compensated power, which is used to avoid the saturation of the PI regulator.

IV. Simulation Results

Simulations are carried in MATLAB/Simulink to validate the proposed control algorithm. The CPL is implemented by using a controllable current source whose current is regulated according to the power of the CPL and dc-bus voltage (output voltage) of the converter. The parameters of the converter are set as follows: switching frequency $f = 20$ kHz, inductance $L = 400$ μH, capacitance $C = 1000$ μF, source voltage $E = 40$ V, output voltage $v = 120$ V, and the nominal power of the CPL is 100 W. The critical value of r'_1 is calculated from (26) to be $r'_{1C} = 0.42$. Then, in the simulation; r'_1 is set as 0.25 ($\xi = 0.6$), 0.42 ($\xi = 1$), and 0.6 ($\xi = 1.4$) to make the system work in the underdamping, critical-damping, and overdamping modes, respectively.

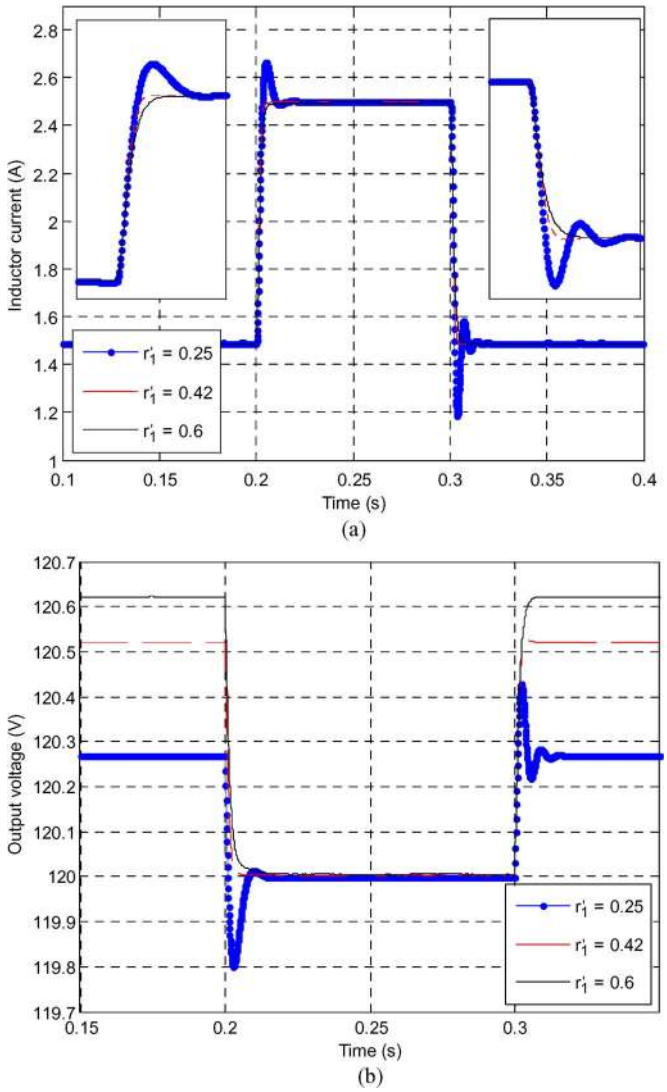

Fig. 5. Simulated inductor current and output voltage responses without the complementary PI controller when the CPL is step changed from 60 to 100 W. (a) Inductor current. (b) Output voltage.

To testify the effectiveness of using the virtual equivalent circuit in Fig. 3 to determine parameter r'_1 of the IDA-PBC, the complementary PI controller is deactivated. In the simulation, the responses of the inductor current and output voltage of the converter are examined when the load is step changed from 60 to 100 W and back to 60 W. Fig. 5 shows the inductor current and the output voltage responses for different values of r'_1, which determines the dynamic characteristic of the system. For instance, $r'_1 = 0.6$ leads to an overdamping system, and there is no overshoot in the inductor current or the output voltage response; when $r'_1 = 0.25$, it is an underdamping system and there are overshoots in both the inductor current and the output voltage responses. In all three cases, the system is stable, which cannot be achieved by using conventional PI controllers due to the negative incremental impedance characteristic of the CPL. However, when the power of the CPL is 60 W, which is lower than its nominal power, the output voltage is slightly higher than

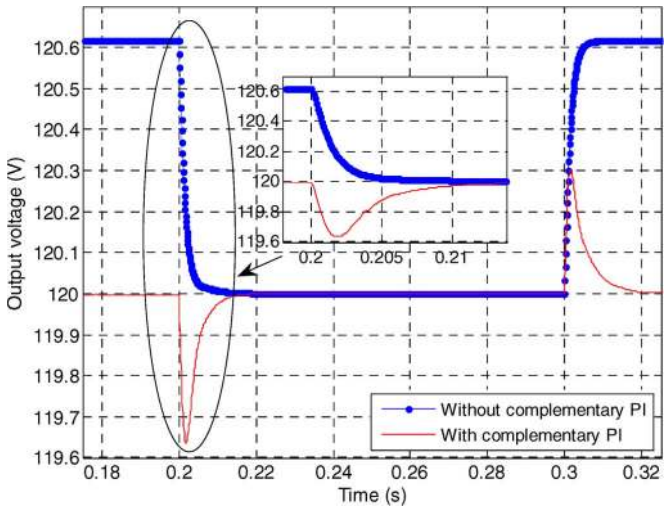

Fig. 6. Simulated output voltage responses of the converter without and with the complementary PI controller ($k_p = 20, k_i = 250 \cdot k_p$) when the CPL is step changed between 60 and 100 W, where $r_1' = 0.6$ in the IDA-PBC.

the desired output voltage of 120 V in all three cases. Such a voltage deviation is caused by the change of the operating point due to the load variation from the operating point (100 W) where the controller is designed. To eliminate the output voltage deviation, a complementary PI controller is used.

Fig. 6 compares the responses of the converter output voltage without and with the complementary PI controller when the CPL is step changed between 60 and 100 W, where $r_1' = 0.6$ in the IDA-PBC. It can be seen that, when the complementary PI controller is not used, the steady-state output voltage changes due to the load variation. When the CPL is 100 W where the IDA-PBC is designed, the steady-state output voltage is maintained at the nominal value of 120 V. However, when the CPL is 60 W, the steady-state output voltage is 120.6 V, which has a 0.6-V deviation from the nominal value. The complementary PI controller is then used with the IDA-PBC to eliminate the steady-state error of the output voltage. The parameters in (27) are set as follows: $e_M = 3$ V, $k_p = 20$, $k_i = 250 \cdot k_p$, and $\Delta P_M = 50$ W. In this case, when the CPL is step changed from 60 to 100 W, the steady-state output voltage is maintained at 120 V accurately after a 10-ms transient. Therefore, the complementary PI controller has effectively eliminated the steady-state error of the output voltage when the load changes.

The proposed control algorithm is also compared with the control algorithm presented in [15] via simulation studies. Fig. 7 shows the simulated inductor current and output voltage responses of the boost dc–dc converter with the control algorithm presented in [15]. The parameters of the control algorithm are set as follows: $r_1 = 2, 4,$ and 6, respectively, and $r_2 = 50$. Large current and voltage overshoots indicate a small damping factor. Therefore, the damping factor increases with the increase in r_1, as shown in Fig. 7. Compared with the proposed control algorithm, which can make the system work in three different modes by using different values of r_1', the control algorithm in [15], however, makes the system work in the underdamping mode only regardless of the value of r_1. Moreover, it should be noted that there is a feasible range for the parameters of the control algorithm in [15]. For example, in this

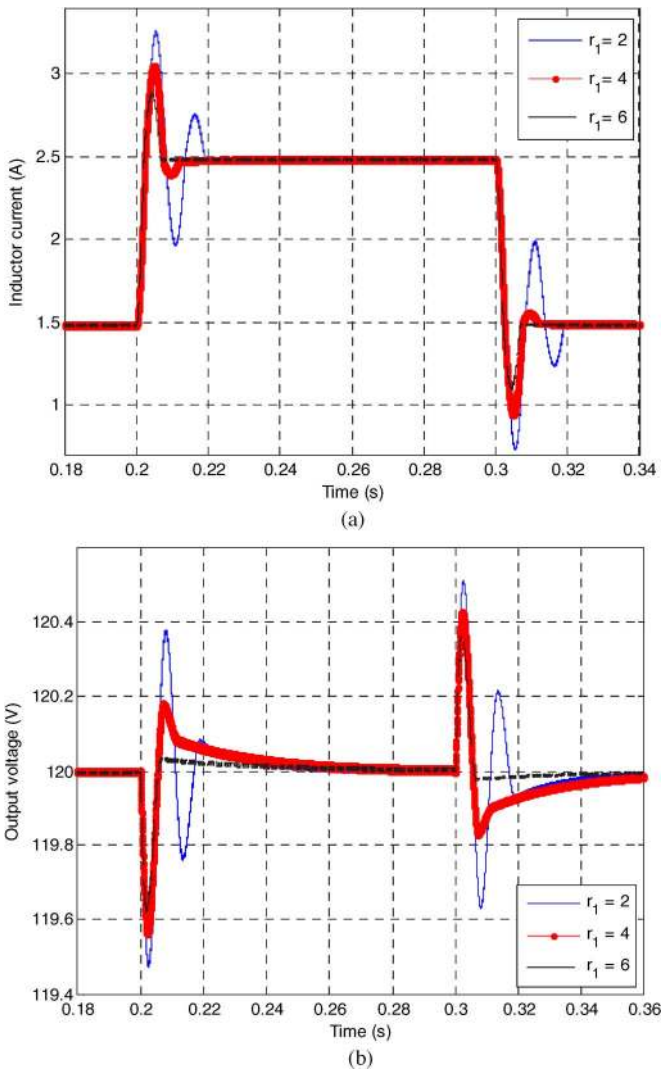

Fig. 7. Simulated current responses using the controller in [15] when the CPL is step changed between 60 and 100 W. (a) Inductor current. (b) Output voltage.

paper the values of r_1 and r_2 should be set less than 7 and larger than 20, respectively; otherwise, it will result in a complex duty ratio, which is not suitable for the converter. The merit of the control algorithm in [15] is that it can eliminate the steady-state output voltage error without using the complementary PI controller. As shown in Fig. 7(b), the steady-state output voltage is always maintained at 120 V in different load conditions. However, the transient lasts 50 ms, which is much longer than the 10-ms transient in Fig. 6. Therefore, the IDA-PBC with the complementary PI controller has faster response than the control algorithm in [15].

V. Experimental Results

The system simulated is constructed in hardware to further validate the proposed control algorithm via experimental studies. Fig. 8 shows the experimental system setup. It consists of the dc–dc boost converter, a dSPACE 1104 board, a converter and dSPACE interface board, a dc source, and a Kikusui Plz664WA programmable dc electronic load, which is used

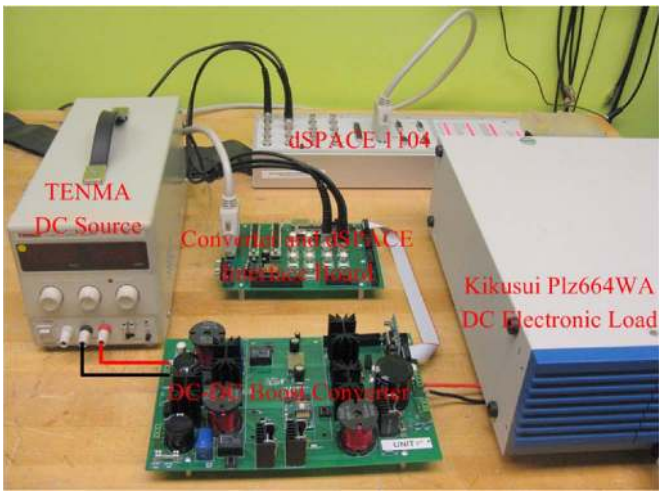

Fig. 8. Experimental system setup.

to emulate the CPL. The control algorithm is implemented in the dSPACE 1104 real-time control platform. The slew rate of the load change is set as 1.2×10^6 W/s instead of infinity in the experiment due to the limitation of the electronic load.

Fig. 9 shows the inductor current (i) and the output voltage (v) responses for different values of r_1' when the load changes from 100 to 60 W without the complementary PI controller. Similar to the simulation results in Fig. 5, when $r_1' = 0.25$, the system is in the underdamping mode, although the measured current and voltage overshoots are smaller than those in the simulation. This is because the damping factor of the system is increased by the parasitic resistance of the inductor, which is connected in series with the virtual resistance r_1', as shown in Fig. 3; whereas such a parasitic resistance is zero in the simulation. When $r_1' = 0.6$, the system is in the overdamping mode, and there is no current or voltage overshoot; which is close to the simulation result. The experimental results again validate the effectiveness of using the virtual equivalent circuit for designing the parameter r_1' of the IDA-PBC. It should be noted that the steady-state inductor current in Fig. 9 is slightly higher than that in Fig. 5. As shown in Fig. 9, when the load is 100 W, the measured inductor current is 2.64 A, which is slightly higher than 2.5 A in Fig. 5. This is because the losses of the converter are neglected in the simulation but cannot be neglected in the experiment. Due to the losses of the converter, it requires a larger current in the experiment than that in the simulation in order to supply the same amount of power to the load. When the load is 60 W, the measured steady-state output voltage corresponding to the underdamping, critical-damping, and overdamping modes are 120.9, 121.3, and 121.4 V, respectively. Such voltage deviations need to be eliminated.

Fig. 10 shows the measured responses of the inductor current (i) and output voltage (v) with the complementary PI controller $(k_p = 20, k_i = 250 \cdot k_p)$ when the CPL is changed from 100 to 60 W and $r_1' = 0.6$. As shown in Fig. 10, the transient state lasts approximately 15 ms, during which the output voltage has a 0.7-V overshoot and then drops back to 120 V. Compared with Fig. 9(c) where the steady-state voltage error is 1.4 V, the steady-state output voltage error is eliminated by using the complementary PI controller.

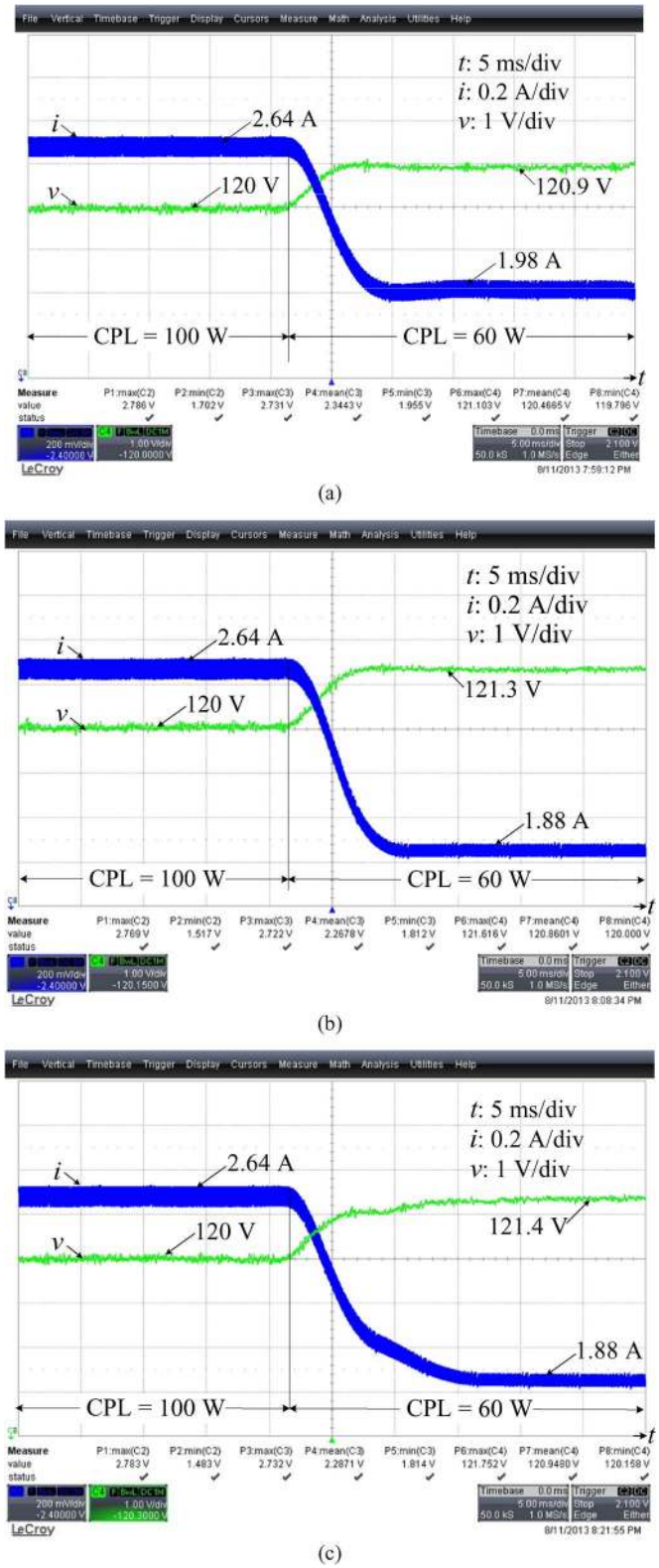

Fig. 9. Measured inductor current (i) and output voltage (v) responses without the complementary PI controller when the CPL is step changed from 100 to 60 W. (a) $r_1' = 0.25$; (b) $r_1' = 0.42$; and (c) $r_1' = 0.6$.

VI. Conclusion

This paper has proposed an IDA-PBC with a complementary PI controller for a dc–dc boost converter with a CPL. A virtual circuit has been introduced for designing the parameters of

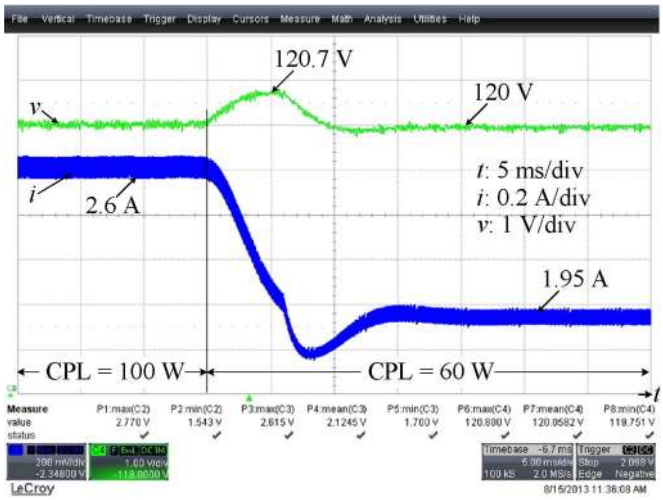

Fig. 10. Measured inductor current (i) and output voltage (v) responses with the complementary PI controller $(k_p = 20, k_i = 250 \cdot k_p)$ when the CPL is step changed from 100 to 60 W and $r_1' = 0.6$ in the IDA-PBC.

the IDA-PBC to effectively control the dc–dc boost converter in underdamping, critical-damping, and overdamping modes. Simulation and experimental studies have been performed to validate the proposed controller. Results have shown that the proposed controller not only ensures the stability but also achieves fast response of the system in different modes. Moreover, the steady-state output voltage error has been eliminated by using the complementary PI controller when the load was changed. The proposed controller is also applicable to other dc/dc converter topologies.

REFERENCES

[1] H. Kakigano, Y. Miura, and T. Ise, "Low-voltage bipolar-type DC microgrid for super high quality distribution," *IEEE Trans. Power Electron.*, vol. 25, no. 12, pp. 3066–3075, Dec. 2010.

[2] H. Kakigano, A. Nishino, Y. Miura, and T. Ise, "Distribution voltage control for DC microgrid by converters of energy storages considering the stored energy," in *Proc. IEEE Energy Convers. Congr. Expo.*, Sep. 2010, pp. 2851–2856.

[3] Y. Ito, Z. Yang, and H. Akagi, "DC microgrid based distribution power generation system," in *Proc. 4th Int. Power Electron. Motion Control Conf.*, Aug. 2004, vol. 3, pp. 1740–1745.

[4] H. Kakigano, M. Nomura, and T. Ise, "Loss evaluation of DC distribution for residential houses compared with AC system," in *Proc. Int. Power Electron. Conf.*, Jun. 2010, pp. 480–486.

[5] K. Doran, F. Barnes, and P. Pasrich, "Smart grid deployment in Colorado: Challenges and opportunities," p. 36, Jun. 2010. [Online]. Available: https://www.smartgrid.gov/sites/default/files/doc/files/Smart_Grid_Deployment_in_Colorado_Challenges_Opportunities_201003.pdf

[6] F. Kanellos, A. Tsouchnikas, and N. Hatziargyriou, "Micro-grid simulation during grid-connected and islanded modes of operation," in *Proc. Int. Conf. Power Syst. Transients*, Jun. 2005, pp. 1–6.

[7] C. Lai, C. Pan, and M. Cheng, "High-efficiency modular high step-up interleaved boost converter for DC-microgrid applications," *IEEE Trans. Ind. Appl.*, vol. 48, no. 1, pp. 161–171, Jan./Feb. 2012.

[8] A. Rahimi and A. Emadi, "An analytical investigation of DC/DC power electronic converters with constant power loads in vehicular power systems," *IEEE Trans. Veh. Technol.*, vol. 58, no. 6, pp. 2689–2707, Jul. 2009.

[9] P. Magne, D. Marx, B. Nahid-Mobarakeh, and S. Pierfederici, "Large-signal stabilization of a DC-link supplying a constant power load using a virtual capacitor: Impact on the domain of attraction," *IEEE Trans. Ind. Appl.*, vol. 48, no. 3, pp. 878–887, May/Jun. 2012.

[10] Y. Zhao, W. Qiao, and D. Ha, "A sliding-mode duty-ratio controller for DC/DC buck converters with constant power loads," *IEEE Trans. Ind. Appl.*, vol. 50, no. 2, pp. 1448–1458, Mar./Apr. 2014.

[11] J. Neely, S. Pekarek, R. DeCarlo, and N. Vaks, "Real-time hybrid model predictive control of a boost converter with constant power load," in *Proc. 25th Appl. Power Electron. Conf. Expo.*, Feb. 2010, pp. 480–490.

[12] A. Kwasinski and P. Krein, "Stabilization of constant power loads in DC-DC converters using passivity-based control," in *Proc. 29th Int. Telecommun. Energy Conf.*, Sep. 30–Oct. 4, 2007, pp. 867–874.

[13] J. Linares-Flores, J. Barahona-Avalos, H. Sira-Ramirez, and M. Contreras-Ordaz, "Robust passivity-based control of a buck–boost-converter/DC-motor system: an active disturbance rejection approach," *IEEE Trans. Ind. Appl.*, vol. 48, no. 6, pp. 2362–2371, Nov./Dec. 2012.

[14] A. Kwasinski and P. Krein, "Passivity-based control of buck converters with constant-power loads," in *Proc. Power Electron. Spec. Conf.*, Jun. 2007, pp. 259–265.

[15] A. Kwasinski and C. Onwuchekwa, "Dynamic behavior and stabilization of DC microgrids with instantaneous constant-power loads," *IEEE Trans. Power Electron.*, vol. 26, no. 3, pp. 822–834, Mar. 2011.

[16] Y. Son and I. Kim, "Complementary PID controller to passivity-based nonlinear control of boost converters with inductor resistance," *IEEE Trans. Control Syst. Technol.*, vol. 20, no. 3, pp. 826–834, May 2012.

[17] S. Glover and S. Sudhoff, "An experimentally validated nonlinear stabilizing control for power electronics based power systems," *Soc. Autom. Eng. J.*, vol. 1, no. 1, pp. 1–10, 1998.

[18] A. Emadi, A. Khaligh, C. Rivetta, and G. Williamson, "Constant power loads and negative impedance instability in automotive systems: definition, modeling, stability, and control of power electronic converters and motor drives," *IEEE Trans. Veh. Technol.*, vol. 55, no. 4, pp. 1112–1125, Jul. 2006.

[19] A. Emadi and M. Ehsani, "Negative impedance stabilizing controls for PWM DC-DC converters using feedback linearization techniques," in *Proc. Intersoc. Energy Convers. Eng. Conf.*, Jul. 2000, pp. 613–620.

[20] R. Ortega, A. van der Schaft, B. Maschke, and G. Escobar, "Interconnection and damping assignment passivity-based control of port-controlled Hamiltonian systems," *Automatica*, vol. 38, no. 4, pp. 585–596, Apr. 2002.

[21] H. K. Khalil, *Nonlinear Systems*, 2nd ed. Englewood Cliffs, NJ, USA: Prentice-Hall, 1996.

Jianwu Zeng (S'10) received the B.Eng. degree in electrical engineering from Xi'an University of Technology, Xi'an, China, in 2004 and the M.S. degree in control science and engineering from Zhejiang University, Hangzhou, China, in 2006. He is currently working toward the Ph.D. degree in electrical engineering at the University of Nebraska–Lincoln, Lincoln, NE, USA.

In 2006, he joined Eaton Electrical (Shenzhen) Company, Ltd., Shenzhen, China, where he was an Electronic Engineer involved in research and development of soft-switching dc–dc converters for uninterruptible power supplies. His research interests include power electronics, renewable energy, and computational intelligence.

Zhe Zhang (S'10) received the B.S. degree in electrical engineering from Xi'an Jiaotong University, Xi'an, China, in 2010. He is currently working toward the Ph.D. degree in electrical engineering at the University of Nebraska–Lincoln, Lincoln, NE, USA.

His current research interests include control of wind energy conversion systems, power electronics, and motor drives.

Wei Qiao (S'05–M'08–SM'12) received the B.Eng. and M.Eng. degrees in electrical engineering from Zhejiang University, Hangzhou, China, in 1997 and 2002, respectively, the M.S. degree in high-performance computation for engineered systems from Singapore-MIT Alliance (SMA), Singapore, in 2003, and the Ph.D. degree in electrical engineering from Georgia Institute of Technology, Atlanta, GA USA, in 2008.

Since August 2008, he has been with the University of Nebraska–Lincoln (UNL), Lincoln, NE USA, where he is currently an Associate Professor in the Department of Electrical Engineering. His research interests include renewable energy systems, smart grids, microgrids, condition monitoring and fault diagnosis, energy storage systems, power electronics, electric machines and drives, and computational intelligence for electric power and energy systems. He is the author or coauthor of three book chapters and more than 130 papers in refereed journals and international conference proceedings.

Dr. Qiao is an Associate Editor of the *IET Power Electronics*, an Associate Editor of the IEEE JOURNAL OF EMERGING AND SELECTED TOPICS IN POWER ELECTRONICS, and the Chair of the Sustainable Energy Sources Technical Thrust of the IEEE Power Electronics Society (PELS). He was an Associate Editor of the IEEE TRANSACTIONS ON INDUSTRY APPLICATIONS during 2010–2013. He was the recipient of a 2010 National Science Foundation CAREER Award, the 2010 IEEE Industry Applications Society (IAS) Andrew W. Smith Outstanding Young Member Award, the 2012 UNL College of Engineering Faculty Research and Creative Activity Award, the 2011 UNL Harold and Esther Edgerton Junior Faculty Award, and the 2011 UNL College of Engineering Edgerton Innovation Award. He has received four best paper awards from the IEEE IAS, IEEE Power Engineering Society, and IEEE PELS.